Water mass transformation and overturning circulation in the Arabian Gulf

Maryam R. Al-Shehhi

Civil and Environmental Engineering, Khalifa University, Abu Dhabi, United Arab Emirates

Hajoon Song*

Department of Atmospheric Sciences, Yonsei University, Seoul, South Korea

Jeffery Scott

Department of Earth, Atmospheric, and Planetary Sciences, Massachusetts Institute of Technology, Cambridge, MA, United States

John Marshall

Department of Earth, Atmospheric, and Planetary Sciences, Massachusetts Institute of Technology, Cambridge, MA, United States

**Corresponding author*: Hajoon Song, hajsong@yonsei.ac.kr

ABSTRACT

We diagnose the ocean's residual overturning circulation of the Arabian Gulf in a high resolution model and interpret it in terms of water-mass transformation processes mediated by air-sea buoyancy fluxes and interior mixing. We attempt to rationalise the complex, 3-dimensional flow in terms of the superposition of a zonal (roughly along-axis) and meridional (transverse) overturning pattern. Rates of overturning and the air-sea fluxes sustaining them are quantified and ranked in order of importance. Air-sea fluxes dominate the budget so that, at zero order, the magnitude and sense of the overturning circulation can be inferred from air-sea fluxes, with interior mixing playing a lesser role. We find that latent heat fluxes dominate the water-mass transformation rate in the interior waters of the Gulf leading to a diapycnal volume flux directed toward higher densities. In the zonal overturning cell, fluid is drawn in from the Gulf of Oman through the Strait of Hormuz, transformed and exits the Strait at depth. Along the southern margin of the Gulf, evaporation plays an important role in the meridional overturning pattern inducing sinking there.

1. Introduction

The water-mass undergoes transformation from one density class to another by the buoyancy fluxes at the sea surface as well as diapycnal mixing. As a result, the volume fluxes arise between density classes and play a fundamental role in the ocean circulation. After Walin (1982) suggested the water-mass transformation framework, it has been serving as a useful tool in understanding the driver of the global and regional ocean circulation (Tziperman 1986; Speer and Tziperman 1992; Garrett et al. 1995; Marshall et al. 1999; Nishikawa et al. 2013; Badin et al. 2013; Abernathey et al. 2016; Cerovečki and Mazloff 2016). This water-mass transformation framework is particularly useful when isopycnals outcrop and multiple layers of fluid have direct pathways between the atmosphere and their interior because the slope of isopycnals can be adjusted subject to the buoyancy forcing and the rate of the water-mass transformation. Additionally, one can anticipate an active water-mass transformation and associated volume fluxes if the buoyancy forcing is considerably large like the Arabian Gulf.

The Arabian Gulf (Gulf hereafter) is a marginal sea of the Arabian Sea that extends from the Sea of Oman in the south to the Shatt-Al-Arab in the north with a length of approximately 1000 km (Fig. 1). It is a shallow, evaporative basin with a depth that rarely exceed 90 m connected to the very much deeper Sea of Oman through the Strait of Hormuz. The restricted exchange with the open ocean through the Strait leads to formation of a saline, dense water-mass which flows out, with fresher waters from the Sea of Oman being drawn in at the surface (see, e.g. Swift and Bower (2003)). This whole system can be thought of as a reverse estuary circulation (Reynolds 1993; Swift and Bower 2003) with the volume flux in $O(0.1\ \text{Sv})$ (Johns et al. 2003; Yao and Johns 2010) and the flushing time of from 3 to 5 years, or even longer than that for the bottom waters (Sadrinasab and Kämpf 2004).

The circulation in the Gulf can be characterized by a cyclonic gyre fed by relatively fresh water from the Gulf of Oman (Reynolds 1993; Johns et al. 2003). While the fluid circles around the Gulf, it loses buoyancy due to excessive evaporation and associated latent heat loss. The desalination plants populated along the south coast further densify the Gulf by brine discharge (Ibrahim and Eltahir 2019). The flow of dense water out of the Gulf is mostly confined to the bottom on the southern side of the channel Swift and Bower (2003).

The cyclonic circulation changes over the course of the year. After the surface current being the strongest in summer, the cyclonic gyre breaks down into smaller mesoscale eddies as evident in the satellite observations and numerical models (Sadrinasab and Kämpf 2004; Thoppil and Hogan 2010; Pous et al. 2015). In winter, the current is the weakest in the year due to the weak stratification and reduced density gradient toward the Gulf (Thoppil and Hogan 2010). The tidal forcing adds barotropic signal to the ocean current and is strong enough to dominate the background current at a given time in the Gulf (Johns et al. 2003) despite the less apparent impact in the average over a few tidal cycles.

As the observational data is limited in the Gulf, the understanding of the circulation is enhanced with the aid of numerical simulations Azhar et al. (2016). Earlier effort focused on the general circulation in the Gulf (Chao et al. 1992), followed by more recent study aiming to investigate the seasonal variability (Kämpf and Sadrinasab 2006), to understand the role of tides (Azam et al. 2006) (Salim et al (2020)), to understand the mesoscale processes (Thoppil and Hogan 2010) and to quantify the budget (Azhar et al. 2016; Xue and Eltahir 2015). However, to the best of our knowledge, the attempt to calculate the overturning circulation in the Gulf and elaborate it using the water-mass transformation framework has not been explored.

In this study we attempt to visualise the complex 3-dimensional circulation patters of the Gulf using zonal and meridional overturning circulation patterns and quantify the relative roles of air-sea heat fluxes and freshwater fluxes in the water mass transformation processes that enable them. We use the MIT ocean circulation model (MITgcm), a versatile, widely-used hydro-dynamical model that solves the incompressible Navier-Stokes equations (Marshall et al. 1997b,a). It has been applied to simulate ocean circulation over a broad range of scales, but has yet to be applied to the special conditions of the Gulf.

Our paper is set out as follows. In Section 2 we describe the design and set-up of our model which is driven by analysed fields in the interior of the domain, by tides imposed at its open boundaries, and run at order 2 km resolution. In Section 3 we describe the resulting water masses and circulation patterns and compare it with observations. In Section 4 we analyse the water-mass transformation processes and overturning circulation patterns associated with our solution, followed by discussion and conclusion in section 5.

2. Design and set-up of a model of the Gulf

a. Global reference model

Our starting point is a high-resolution global configuration of the MITgcm, the so-called LLC4320 simulation (Rocha et al. 2016; Torres et al. 2018). The global setup employs a latitude/longitude/polar cap (LLC) configuration on a Arakawa-C grid using a nominal horizontal grid spacing of 1/48Âř; in practice, the grid has an almost uniform meridional and zonal spacing of approximately 2.0 km in the Gulf region, but varies between 0.8 km and 2.2 km over the globe. There are 90 vertical levels, ranging from a thickness of 1 m at the surface to 480 m at depth with a linearized implicit free surface. The model is integrated at every 25 seconds with a seventh-order monotonicity-preserving advection scheme (Daru and Tenaud 2004) and no explicit horizontal diffusivity. Horizontal viscosity and vertical mixing is parameterized using a biharmonic “modified

Leith viscosity” with a vertical viscosity of 5.4×10^{-4} m^2 s^{-1} and the K-profile parameterization (KPP; Large et al. (1994)) with a background diffusivity of 5.4×10^{-7} m^2 s^{-1}, respectively. No-slip boundary conditions on the bottom and side are used.

The LLC4320 simulation was run for the calendar period September 13, 2011 through November 15, 2012, with initial conditions taken from a series of hierachy simulateion started from the ECCO2 state estimation (Menemenlis et al. 2008). It was forced at the surface by six-hour European Centre for Medium-Range Weather Forecasting (ECMWF) atmospheric operational model analysis at 0.14Âř resolution, (roughly 15 km) using bulk formulae following Large and Pond (1981). A synthetic atmospheric surface pressure field consisting of 16 tidal forcing constituents was used to dynamically mimic tidal forcing (Wang et al. 2018). Monthly river runoff was derived from Large and Nurser (2001) (see also Stammer et al., 2004).

b. Embedded model of the Gulf and Sea of Oman

Our study region is the Gulf and its connection to the Sea of Oman, as shown in Fig. 1. A regional model is configured and embedded in the global model described above.Starting from the global model bathymetry, modifications were made to more accurately represent the coastlines in the Gulf. A 2 arc-minute resolution bathymetry, yielding approximately 3.5 km in the Gulf, is employed based on Smith and Sandwell (1997). The model comprises 832×480 cells, and uses the same vertical resolution as the global model, except only 83 levels were required to represent the deep ocean in the Sea of Oman; in the relatively shallow Gulf, only the uppermost 22 vertical levels are active. The surface forcing is identical to that of the global model and used ECMWF data for the full calendar year 2012. However, a custom monthly river freshwater outflow data set (capturing the discharge of the Shatt Al-Arab, Mand, Hindijan and Hilieh rivers) was configured for our modified bathymetry based on Alosairi and Pokavanich (2017). For computational efficiency, the model time step was increased from 25 seconds to 60 seconds, leading to only minor differences in short test simulations. Open boundary conditions (currents, salinity, temperature, and sea surface height) were imposed at the southern and eastern boundaries, obtained from the global run. To improve upon the representation of the tides presented to our regional model from the global model, 5-day running means of open boundary data from the global model were calculated, filtering out the tidal forcing signal. New tidal forcing components were then constructed, based on Egbert and Erofeeva (2002) comprising the M2, S2, K2, K1, O1, and P1 tidal constituents, and were added to the southern and eastern open boundary conditions. After initialized using the global run, the Gulf model was run on for a total of eight years using repeating 2012 year forcing; the first six years were considered to be the spin-up period and the last two years used for the analyses presented here.

A discussion of the skill of the model in capturing tides in the interior of our domain is given in Salim et al (2020), where a detailed comparison with observations from observations from tide gauges distributed around the Gulf is presented. Here we focus on the general circulation aspects of the solution and in particular the water mass transformation and overturning therein.

3. Modeled circulation in the Gulf

a. Temperature and Salinity structure

The solution is compared to in situ observations of temperature and salinity taken from the Master Oceanographic Observations Data Set (MOODS) (Alessi et al. 1999). The data spans the period of the 1940s up to the 1990s and has a rather inhomogeneous distribution in both time and space. We therefore use seasonal-mean vertical profiles of temperature and salinity averaged within the black boxes shown in Fig. 1, following the study of Swift and Bower (2003). Although the observations remain rather sparse even after such temporal and spatial averaging, they clearly document significant seasonality in the stratification of the Gulf.

The observations reveal that in summer the Gulf is strongly stratified (Fig. 2(a,c,e)). The temperature can exceed 30°C at the surface yet is colder than 20° below 100 m. The salinity increases with depth but relatively slowly compared with the temperature. The vertical structure of density closely follows that of temperature, showing that temperature plays the dominant role in setting stratification. In winter, in contrast, the temperature becomes vertically uniform (Fig. 3(a)). Colder temperatures can be found toward the western margin of the Gulf where it is below 19°C. The vertical distribution of salinity is less homogeneous than that of temperature and bottom waters are particularly salty in winter exceeding concentrations of 40 psu (Fig. 3(c)). Since cold and salty waters are located at the innermost region of the Gulf, the density typically increases toward the bottom of the northern end of the Gulf (Fig. 3(e)).

Our numerical solution exhibits broad similarities with the observations, but also differences. It has clear seasonality, with highly stratified water in summer whilst relatively homogeneous in winter. The solution does not capture the water mass whose salinity is greater than 40 psu near the bottom, nor the increasing salinity trend toward the northern end of the Gulf (Fig. 2(d) and 3(d)). This leads to an underestimate of the density in these regions (Fig. 2(f) and 3(f)). The simulated temperature is slightly colder in summer and warmer in winter (Fig. 2(b) and 3(b)) relative to the observations, but the difference is small compared to the magnitude of the seasonal cycle and internal variability. Given that our solution is driven by repeated surface forcing from a particular year whilst the observations span over 50 years, and the river runoff varies from year to year, it is encouraging that the spatial distribution of density is broadly comparable between the observations and model. This suggests that there is merit in going on to further analyze the general circulation in the Gulf.

b. Horizontal circulation patterns

Surface currents in the Gulf are characterized by a cyclonic gyre. Inflow through the Strait of Hormuz, and the southeast flow from the central region of the Gulf toward the Strait, are present in both seasons (Fig. 4(b,d)). In summer, the surface flow is more dynamic than in winter, with a northwest current near the northern coast of the Gulf as well as southward flow along 50°E. These horizontal circulation patterns can partially be explained by the pattern of prevailing wind stress (Fig. 4(a,c)). In summer, the southeastward wind stress is the strongest in the northern Gulf, and surface flow is generally to the southeast, carrying relatively fresh water from river runoff entering on the northern coast of the Gulf (Fig. 2(d)). In winter, in contrast, the maximum wind stress is found over the center of the Gulf and is responsible for the southeast surface flow there. In wintertime the surface flow of the northern Gulf, and the inflow coming through the Strait of Hormuz along the northern coast, both significantly weaken. Cyclonic flow is much less distinct than in the summer and shifted to the south. It is likely that the former is caused by the wintertime wind stress which is directed opposite to the surface flow, whilst the latter is a consequence of a thicker surface layer with relatively uniform density at the northern end of the Gulf (Fig. 3(e,f)).

The barotropic streamfunction for the depth-integrated circulation in the Gulf has a dipole pattern, as can be seen in Fig.5. Positive values are found over a broad area in the southern part of the Gulf, while negative values are found in a relatively narrow band near the northern coastal region. This indicates broad cyclonic (counterclockwise) circulation in the southern Gulf with narrow anticyclonic (clockwise) circulation to the north of it. Sandwiched between these two patterns is the inflow through the Strait of Hormuz which extends westwards to 52°E or so. The vertical section of zonal velocity at the Strait (inset in Fig. 5) reveals that the inflow extends mid-way across, from the surface to the ocean floor, with speeds of $O(0.1 \text{ m s}^{-1})$. The streamfunction also suggests outflow near the southern and northern ends of the Strait of Hormuz. The existence of the outflow near the southern end of the Strait is consistent with previous observational studies (e.g. Johns et al. 2003), but the outflow near Qeshm Island at the northern end is also a notable feature. The core of the outflow is bottom-intensified, as seen in the observations (Schott and McCreary 2001). Toward the north-western end of the Gulf, there is little evidence of a structured barotropic flow in the annual mean.

4. Water-mass transformation and overturning circulation

As described in the introduction, properties of fluid coming in through the Strait of Hormuz are transformed by air-sea fluxes and mixing within the Gulf, so that fluid exiting from the Strait has properties which are different from that on entry. We now analyse this water-mass transformation process in our Gulf model following the framework set out in Walin (1982) and Marshall et al. (1999). This can be used to elegantly infer and quantify the processes sustaining the overturning circulation.

a. Theoretical framework

Following the line of reasoning in Marshall et al. (1999), let us consider the volume of fluid within a certain density class, $\mathcal{R}_\sigma(\sigma, t)$, as sketched in Fig.6 which shows potential density layers centered around σ outcropping at the surface within the Gulf (say) and extending back out in to the Gulf of Oman. The volume $\mathcal{R}_\sigma(\sigma, t)$ can be changed by a diapycnal volume flux, $A(\sigma, t)$, normal to isopycnal surfaces defined in terms of the fluid velocity ($\mathbf{v}$) and the isopycnal velocity ($\mathbf{v}_\sigma$) normal to the σ surfaces:

$$A(\sigma, t) = \iint_{\mathcal{A}_\sigma(\sigma,t)} (\mathbf{v} - \mathbf{v}_\sigma) \cdot \hat{\mathbf{n}}_\sigma d\mathcal{A}, \tag{1}$$

where $\mathcal{A}_\sigma(\sigma,t)$ is the area of isopycnal surface and $\hat{\mathbf{n}}_\sigma$ is a unit vector normal to the isopycnal surface directed from low to high values. As defined in Eq. (1), $A(\sigma,t)$ is positive when there is a flux toward higher density since σ increases downwards, as sketched in Fig.6.

The evolution of σ itself is governed by the equation:

$$\frac{\partial\sigma}{\partial t} = -\nabla\cdot(\mathbf{N}_\sigma + \sigma\mathbf{v}) \tag{2}$$

where $\mathbf{N}_\sigma$ is the non-advective flux of σ, and $\sigma\mathbf{v}$ is the advective flux. As first shown by Walin (1982), $A(\sigma,t)$ can be precisely related to $B(\sigma,t)$, the non-advective supply of buoyancy to the control volume $\mathcal{R}(\sigma,t)$, as follows (using the notation of Marshall et al, 1999)

$$A(\sigma,t) = \frac{\partial B(\sigma,t)}{\partial\sigma} \tag{3}$$

where

$$B(\sigma,t) = -\iiint_{\mathcal{R}_\sigma(\sigma,t)} \nabla\cdot\mathbf{N}_\sigma dV \tag{4}$$

depends on $\mathbf{N}_\sigma$ acting on the boundaries of $\mathcal{R}_\sigma$.

Separating Eq. (3) in to a part due to air-sea fluxes and a part due to diffusive, non-advective fluxes acting in the interior ocean, it can be written:

$$A = F - \frac{\partial D}{\partial\sigma}, \tag{5}$$

where

$$F = \frac{\partial B_s(\sigma,t)}{\partial\sigma} \tag{6}$$

depends only on surface fluxes and

$$D = \iint_{\mathcal{A}\sigma} \mathbf{N}_\sigma\cdot\hat{\mathbf{n}}_\sigma d\mathcal{A}, \tag{7}$$

depends on diffusive fluxes within the ocean.

The quantity F is called the 'transformation' and given by

$$B_s(\sigma,t) = -\frac{\rho_0}{g}\iint_{\mathcal{A}_s(\sigma,t)} \mathcal{B}_s d\mathcal{A}, \tag{8}$$

where $\mathcal{A}_s(\sigma,t)$ is the area of the sea surface with the density interval around σ at time t and

$$\mathcal{B}_s = \frac{g}{\rho_0}\left(\frac{\alpha}{c_w}(Q_{SW}+Q_{LW}+Q_L+Q_S)+\rho_0\beta S(E-P-R)\right) \tag{9}$$

is the air-sea buoyancy flux made up of its heat (first term in brackets on the right-hand side, and freshwater (second term in brackets on the right-hand side) contributions. Here, ρ_0 is the reference density, α is the thermal expansion coefficient for sea water, c_w is the heat capacity of water, Q_{SW}, Q_{LW}, Q_L, and Q_S are the heat flux due to shortwave radiation, longwave radiation, latent heat and sensible heat, respectively, β is the haline contraction coefficient, and E, P and R are evaporation, precipitation and river runoff, respectively. Note that in the above A and F have units of m^3 s^{-1}, B_s has units of kg s^{-1} m^{-2} and $\mathcal{B}_s$ has units of m^2 s^{-3}.

At the surface of the ocean, if outcropping buoyancy surfaces lose increasingly more buoyancy at higher density classes, then $\frac{\partial B_s(\sigma,t)}{\partial\sigma} > 0$, and F is in the sense to induce a positive A: in the absence of diffusive processes, fluid moves to heavier density classes. In this way, computing F for each density class at the surface enables us to probe the role of air-sea fluxes in sustaining the overturning circulation.

b. Diagnosis of water mass transformation in our Gulf model

We use MITgcm's capability to compute water-mass transformation rates as a function of density class. These diagnostics are obtained through use of the LAYERS package in which the theoretical framework described above is put in to practice (see Abernathey et al. 2016). Our layers are chosen to range from 22 to 42.1 kg m^{-3} with an interval of 0.15 kg m^{-3}. This encompasses most of the water-mass in the domain, but occasionally density variations exceed this range: in summer when evaporation increases density beyond 42.1 kg m^{-3} and in winter when freshwater input near the rivers lowers the density below 22 kg m^{-3}. If this occurs, those water masses which lie outside our chosen range are merged to the closest density bin. LAYERS also computes the velocity within isopycnal layers allowing us to directly estimate the overturning circulation in the Gulf and Sea of Oman, as described in the section 4.3 below.

As shown in Fig. 7(a), annually-averaged water-mass transformation rates, weighted by grid area, show that surface fluxes act to induce a flow toward higher density classes. Since surface waters in the Gulf are generally denser than in the Sea of Oman, this implies water is being drawn in to the Gulf by air-sea transformation within the Gulf. This is in contrast to the rather small transformation rates in the Gulf of Oman. The central Gulf near the northern coast has the most active water-mass transformation, with values exceeding 100 m^3 s^{-1}. Here the contribution from the net heat flux dominates that from the freshwater flux (Fig. 7(b,c)). Heat loss associated increases the surface density resulting in a water-mass transformation rate which is positive over the interior of the Gulf. This should be contrasted with the transformation rate near the southern coast where evaporation, E, results in a net positive water-mass transformation in the Gulf (Fig. 7(a,c)), despite the warming effects of the net heat flux there (see Fig. 7(b)). In broad summary, the net effect of air-sea fluxes over the Gulf is to draw light water in through the Strait of Hormuz and make it denser.

The water-mass transformation rate in the Gulf can be further visualized by dividing the Gulf on through the Strait of Hormuz in to narrow bands which are ascribed numbers from 0 to 100 starting from the innermost region in the Gulf out through the Strait in to the Gulf of Oman (Fig. 7(a)). The transformation, F in Eq. (6), is then averaged over these bands to yield Fig. 8 where the various contributions of the surface flux components – see Eq. (9) – separated out.

Fig. 8 confirms our notion that the Arabian Gulf is a marginal sea in which evaporation exceeds precipitation thus increasing the density of surface waters. The Gulf also receives abundant shortwave solar radiation which warms the sea surface releasing sensible heat into the atmosphere, increasing surface density in the Gulf. However, sensible heat loss occurs at a rate which is almost two orders of magnitude smaller than the warming shortwave contribution. It is clear from Fig. 8 that this gain is largely balanced by heat loss from outgoing long-wave radiation and latent heat. Indeed latent heat loss is the single largest contributor to a positive water-mass transformation and, as presented in Fig.8, has 5 times greater impact than evaporation in increasing surface density.

Our simulation has a linear free surface formulation which introduces a surface correction term for the local conservation of tracers (Campin et al. 2004). The correction term has the effect of reducing surface salinity over most of the Gulf. Near the mouth of rivers where there is considerable freshwater input, however, the correction term is positive. The correction term for temperature tends to increase the density, but the sum of both salt and temperature correction terms has a net negative effect on transformation rate (Fig. 8). Although these correction terms are not small enough to be neglected, we will not discuss them further since they are not directly related to surface fluxes.

The volume flux across isopycnals may converge or diverge fluid in to a certain density class, leading to inflation or deflation of the volume of fluid within the layer. The formation rate – the volume squeezed in to a layer – can be computed as $\partial A/\partial\sigma$ (Marshall et al. 1999). The water-mass transformation rate in Fig. 8 is plotted against distance rather than density as in (Abernathey et al. 2016), because the surface density spatial distribution does not carry much geographical information; the same density can be found in multiple places. Although, for this reason, the formation rate cannot be obtained quantitatively from Fig. 8, we can still qualitatively describe it by inspecting the transformation rate and surface density together.

The transformation rate in the Gulf is positive, suggesting that the volume flux is directed toward water-masses of higher density which are typically found at the center of the Gulf. The surface density shows a rather complicated distribution (the green dashed line in Fig. 8). There are at least two distinct peaks in the Gulf; one near bin number 30 and the other one near 45. The density is relatively low northwest of the center where the water-mass transformation rate remains positive. This implies that there is a convergence of A near the center of the Gulf. There is also a convergence of A toward the innermost part of the Gulf where there is a rapid increase of the transformation rate and a decrease of density (Fig. 8). At these sites, the convergence of A results in a creation of water-mass at that particular density and downwelling of surface water. The geometry of the isopycnals is broadly consistent with this interpretation, as we describe in c.

The density at the surface can also be changed by diapycnal diffusive flux occurring within the ocean (Marshall et al. 1999). The diapycnal diffusive flux can also be partitioned into heat and salt diffusion, and both make a positive contribution to the transformation (Fig. 9). The transformation rates due to these diffusive fluxes make a generally smaller contribution than surface fluxes. However, this is not true everywhere. For example, the diapycnal diffusive salinity flux approaches 100 m^3 s^{-1} near the river mouths along the northern coast and the innermost parts of the Gulf (Fig. 9(b)). As the rivers provide freshwater to the Gulf, the salinity difference between the surface of the ocean and below is considerable at these sites and vertical mixing can acts to increase the density, making a positive contribution to water-mass transformation.

c. Overturning circulation in the Gulf

We can analyze the annually-averaged residual overturning circulation in the Gulf and the Gulf of Oman by making use of the currents projected along isopycnals, provided by the LAYERS diagnostic package of MITgcm and then re-mapped in to z-space for viewing (Fig. 10). Note that the diagnostics are computed on-line and thus includes transports of all resolved scales (including tides and eddies) – in particular is not the Eulerian-mean overturning circulation but rather the residual circulation, as discussed in the context of the Antarctic Circumpolar Current in, for example, Marshall and Radko (2003). We explore both zonal and meridional overturning cells. The streamfunction is defined such that there is counterclockwise circulation around negative values.

The overturning circulation in the zonal direction highlights the flow through the Strait of Hormuz where the inflow and outflow is found at the surface and near the bottom, respectively (Fig. 10(a)). The sense of the zonal overturning circulation confirms inflow of relatively fresh water from the Gulf of Oman into the Arabian Gulf, consistent with our diagnosis of the positive water-mass transformation rate shown in Fig. 8 and the inset of Fig. 5. The overturning circulation is considerably weaker within the Gulf than outside it. The zonal residual streamfunction indicates that the surface inflow weakens and subducts at approximately 53°E. This characteristic of the surface current is also consistent with a convergence of the water-mass transformation rate (Fig. 8) seen near bin number 45 corresponding to roughly 53°E, in the central Gulf. The outflow at depth enters the Gulf of Oman and finds its neutral level near 200 m or so and spreads eastwards. There is an upwelling near 60°E induced by monsoon winds; the southwesterly wind in the summer is stronger than the northeasterly wind in winter, leading to net upwelling (Fig. 4(a,c)).

The overturning circulation further inside the Gulf is generally negative (Fig. 10(b)). Negative values north of 27°N suggests the surface current is directed toward the center of the Gulf while that to the south of 26°N indicates surface southward flow that sinks to the bottom at the southern coast. The streamfunction to the north of 27°N is again consistent with the water-mass transformation rate whose positive values indicates a volume flux toward the center of the Gulf. The circulation pattern in the southern part of the Gulf also agrees with both the sense of the seasonal surface current and the barotropic streamfunction (Fig. 4 and 5). Interestingly, the water-mass transformation near the southern coast is mainly associated with freshwater flux (Fig. 7(c)), as discussed above.

The density decreases toward the innermost part of the Gulf where isopycnals bend downward, indicating downwelling (Fig. 10). Although our density bias in the innermost part of the Gulf might amplify this feature, observations also show the relatively low density water at the very end of the Gulf with a doming of isopycnals, especially in the summer (Fig. 7 in (Swift and Bower 2003)). Our water-mass transformation rate diagnostic is also suggestive of downwelling. As discussed in Section 4, the density increases toward the center of the Gulf while the water-mass transformation rate is positive, resulting in a positive water formation rate ($\partial A/\partial\sigma > 0$) (Fig. 8). This downwelling is better shown in the meridional overturning streamfunction where it is evident near 30°N (Fig. 10(b)). The consistent results between the overturning circulation and water-mass transformation rate demonstrate a satisfying and consistent connection between air-sea buoyancy fluxes and the general circulation in the Gulf.

5. Discussion and Conclusions

The Arabian Gulf is a semi-closed evaporative basin in which relatively fresh water is supplied near the surface through the Strait of Hormuz while salty water exits the Gulf at depth. The differing salinities between the inflow and outflow at the Strait suggests that water-mass transformation must be positive within the Gulf with the density of the water being increased. Surface fluxes are responsible for this densification, but the detailed processes of water-mass transformation and resulting overturning circulation are complex and not fully documented or understood. We have made use of the MITgcm and its diagnostic capabilities (Abernathey et al. 2016; Doddridge et al. 2019) to explore these processes in a novel and hopefully illuminating way.

The circulation derived from our 1/48° resolution model is depicted schematically in Fig. 11. The surface flow is characterized by inflow through the Strait of Hormuz and cyclonic circulation on the eastern margin of the Gulf feeding outflow toward the Gulf of Oman. The northwest region of the Gulf comprises a current flowing toward the center of the Gulf. Formation of bottom water occurs in the central Gulf and southern coastal regions. In the central Gulf, air-sea heat flux is the main cause of densification. Surface density decrease due to solar heating is counterbalanced by both upward longwave radiation and latent heat loss. In particular, latent heat loss is the largest contributor to density increase and contributes five times as much to water-mass transformation than does evaporation (Fig. 8). Densification of surface waters close to the southern coast, instead, is mainly driven by evaporation (Fig. 7) and sinks to depth. Some of this heavy water near the ocean floor returns back to the northwest part of the Gulf, especially in summer when the water is stratified (not shown). However, much of it exits the Gulf through the southern portion of the Strait of Hormuz, finding its level at 200 m or so in the Gulf of Oman.

The circulation within the Gulf is in accord with expectations based on water-mass transformation theory (Walin 1982; Marshall et al. 1999). Positive water-mass transformation rates due to surface fluxes (Fig. 7) implies a convergence of volume flux toward higher densities at the center of the Gulf. Water-mass transformation rates remain positive while, at the same time, the surface density decreases northwestward toward the innermost part of the Gulf. This implies that the surface volume flux is directed southeastward, which is consistent with the circulation pattern found in that region. We thus observe surface volume fluxes converging from both sides toward the center of the Gulf supporting subsequent downwelling where the density is higher than elsewhere.

The annually averaged volume flux through the Strait of Hormuz in our calculations is somewhat larger than 0.1 Sv, at the lower limit of the previously reported values (Johns et al. 2003). A relatively lower volume flux might be due to an underestimation of salinity or a consequence of seasonality – the streamfunction reaches 0.18 Sv in winter (not shown).

Our study suggests that, because the contribution to the transformation rate by interior diffusive fluxes are so much smaller than that due to air-sea fluxes, the transformation can be inferred to a good approximation directly from air-sea fluxes. This implies that any changes in air-sea fluxes will modify the overturning circulation. The 2-m temperature over the Gulf shows a positive trend ($\approx$ 0.3 °C/decade), (Patlakas et al. 2019), and sea surface temperatures are also warming (Shirvani et al. 2015; Noori et al. 2019). Along with this warming trend, the freshwater flux also varies in time (Campos et al. 2020). The warming trend, coupled with a net negative freshwater flux ($E-P$) over the Gulf, will likely continue in to the future (Kirtman et al. 2013). Wind changes may also be important since they are intimately involved in setting patterns and magnitudes of surface fluxes. Our study therefore sets out a clear analysis method for understanding and perhaps predicting such changes. This will be the topic of future research.

Finally, our experiment design also provides a comprehensive framework from which to compute the impact of desalination plants on oceanic circulation in the Gulf. The lives of people living around the Gulf depend on a supply of fresh water provided by desalination facilities. During the desalination process, freshwater is removed from sea water and brine is discharged back to the Gulf. This can result in an increase in salinity which is twice as high as the water drawn in to the facilities (Bashitialshaaer et al. 2011). The discharge typically occurs near the surface and acts as a negative freshwater flux (Ibrahim and Eltahir 2019). According to the water-mass transformation framework employed here, desalination plants will contribute to an enhancement of water-mass formation near the coastal region inducing stronger sinking. This will likely strengthen the overturning circulation and enhance the inflow through the Strait of Hormuz. As more desalination facilities are anticipated in the future, likely changes in overturning circulation could perhaps be estimated using the approach outlined here.

Acknowledgments. H.S. acknowledges the support by National Research Foundation of Korea (NRF) grant (NRF-2019R1C1C1003663) and Yonsei University Future-leading Research Initiative of 2020-22-0114. M.A., J.M. and J.S. acknowledges Khalifa University for its generous financial support and Prof. Hosni Ghedira for the access to his laboratory facilities.

Data availability statement. The full LLC4320 model setup with compile-time and run-time parameters can be found at `http://wwwcvs.mitgcm.org/viewvc/MITgcm/MITgcm_contrib/llc_hires/llc_4320/`.

References

Abernathey, R. P., I. Cerovecki, P. R. Holland, E. Newsom, M. Mazloff, and L. D. Talley, 2016: Water-mass transformation by sea ice in the upper branch of the Southern Ocean overturning. *Nat. Geosci.*, **9 (8)**, 596–601, doi:10.1038/ngeo2749.

Alessi, C. A., H. D. Hunt, and A. S. Bower, 1999: Hydrographic data from the us naval oceanographic office: Persian gulf, southern red sea, and arabian sea 1923-1996hydrographic data from the us naval oceanographic office: Persian gulf, southern red sea, and arabian sea 1923-1996. Tech. rep., Woods Hole Oceanographic Institution, Woods Hole, MA. US.

Alosairi, Y., and T. Pokavanich, 2017: Residence and transport time scales associated with Shatt Al-Arab discharges under various hydrological conditions estimated using a numerical model. *Mar. Pollut. Bull.*, **118 (1–2)**, 85–92, doi:10.1016/j.marpolbul.2017.02.039.

Azam, M. H., W. Elshorbagy, T. Ichikawa, T. Terasawa, and K. Taguchi, 2006: 3D Model Application to Study Residual Flow in the Arabian Gulf. *J Waterw. Port. Coast.*, **132 (5)**, 388–400, doi:10.1061/(ASCE)0733-950X(2006)132:5(388).

Azhar, M. A., M. Temimi, J. Zhao, and H. Ghedira, 2016: Modeling of circulation in the Arabian Gulf and the Sea of Oman: Skill assessment and seasonal thermohaline structure. *J. Geophys. Res. Oceans*, **121 (3)**, 1700–1720, doi:10.1002/2015JC011038.

Badin, G., R. G. Williams, Z. Jing, and L. Wu, 2013: Water Mass Transformations in the Southern Ocean Diagnosed from Observations: Contrasting Effects of Air–Sea Fluxes and Diapycnal Mixing. *J. Phys. Oceanogr.*, **43 (7)**, 1472–1484, doi:10.1175/JPO-D-12-0216.1.

Bashitialshaaer, R., K. M. Persson, and M. Aljaradin, 2011: Estimated future salinity in the Arabian Gulf, the Mediterranean Sea and the Red Sea consequences of brine discharge from desalination. *Int. J. Acad. Res.*, **3 (1)**, 133–140.

Campin, J.-M., A. Adcroft, C. Hill, and J. Marshall, 2004: Conservation of properties in a free-surface model. *Ocean Modell.*, **6 (3)**, 221 – 244, doi:https://doi.org/10.1016/S1463-5003(03)00009-X.

Campos, E. J. D., A. L. Gordon, B. Kjerfve, F. Vieira, and G. Cavalcante, 2020: Freshwater budget in the Persian (Arabian) Gulf and exchanges at the Strait of Hormuz. *PLoS ONE*, **15 (5)**, e0233 090, doi:10.1371/journal.pone.0233090.

Cerovečki, I., and M. R. Mazloff, 2016: The Spatiotemporal Structure of Diabatic Processes Governing the Evolution of Subantarctic Mode Water in the Southern Ocean. *J. Phys. Oceanogr.*, **46 (2)**, 683–710, doi:10.1175/JPO-D-14-0243.1.

Chao, S.-Y., T. W. Kao, and K. R. Al-Hajri, 1992: A numerical investigation of circulation in the Arabian Gulf. *J. Geophys. Res. Oceans*, **97 (C7)**, 11 219–11 236, doi:10.1029/92JC00841.

Daru, V., and C. Tenaud, 2004: High order one-step monotonicity-preserving schemes for unsteady compressible flow calculations. *J. Comput. Phys.*, **193 (2)**, 563–594, doi:10.1016/j.jcp.2003.08.023.

Doddridge, E. W., J. Marshall, H. Song, J.-M. Campin, M. Kelley, and L. Nazarenko, 2019: Eddy compensation dampens Southern Ocean sea surface temperature response to westerly wind trends. *Geophys. Res. Lett.*, **46 (8)**, 4365–4377, doi:10.1029/2019GL082758.

Egbert, G., and S. Erofeeva, 2002: Efficient inverse modeling of barotropic ocean tides. *J. Atmos. Oceanic Technol.*, **19**, 183–204, doi:10.1175/1520-0426(2002)019<0183:EIMOBO>2.0.CO;2.

Garrett, C., K. Speer, and E. Tragou, 1995: The Relationship between Water Mass Formation and the Surface Buoyancy Flux, with Application to Phillips' Red Sea Model. *J. Phys. Oceanogr.*, **25 (7)**, 1696–1705, doi:10.1175/1520-0485(1995)025<1696:TRBWMF>2.0.CO;2.

Ibrahim, H. D., and E. A. B. Eltahir, 2019: Impact of Brine Discharge from Seawater Desalination Plants on Persian/Arabian Gulf Salinity. *J. Environ. Eng.*, **145 (12)**, 04019 084, doi:10.1061/(ASCE)EE.1943-7870.0001604.

Johns, W. E., F. Yao, D. B. Olson, S. A. Josey, J. P. Grist, and D. A. Smeed, 2003: Observations of seasonal exchange through the Straits of Hormuz and the inferred heat and freshwater budgets of the Persian Gulf. *J. Geophys. Res. Oceans*, **108 (C12)**, doi:10.1029/2003JC001881.

Kämpf, J., and M. Sadrinasab, 2006: The circulation of the Persian Gulf: a numerical study. *Ocean Sci.*, **2 (1)**, 27–41, doi:https://doi.org/10.5194/os-2-27-2006.

Kirtman, B., and Coauthors, 2013: Near-term climate change: Projections and predictability. *Climate Change 2013: The Physical Science Basis, Contribution of Working Group I to the Fifth Assessment Report of the Intergovernmental Panel on Climate Change*, T. Stocker, D. Qin, G.-K. Plattner, M. Tignor, S. Allen, J. Boschung, A. Nauels, Y. Xia, V. Bex, and P. Midgley, Eds., Cambridge University Press, Cambridge, United Kingdom and New York, NY, USA.

Large, W. G., J. McWilliams, and S. Doney, 1994: Oceanic vertical mixing: A review and a model with nonlocal boundary layer parameterization. *Rev. Geophys.*, **32 (4)**, 363–403.

Large, W. G., and S. Pond, 1981: Open ocean momentum flux measurements in moderate to strong winds. *J. Phys. Oceanogr.*, **11**, 324–336.

Marshall, J., A. Adcroft, C. Hill, L. Perelman, and C. Heisey, 1997a: A finite-volume, incompressible Navier Stokes model for studies of the ocean on parallel computers. *J. Geophysical Res.*, **102 (C3)**, 5753–5766.

Marshall, J., C. Hill, L. Perelman, and A. Adcroft, 1997b: Hydrostatic, quasi-hydrostatic, and nonhydrostatic ocean modeling. *J. Geophysical Res.*, **102 (C3)**, 5733–5752.

Marshall, J., D. Jamous, and J. Nilsson, 1999: Reconciling thermodynamic and dynamic methods of computation of water-mass transformation rates. *Deep-Sea Res. I*, **46 (4)**, 545–572.

Marshall, J., and T. Radko, 2003: Residual-Mean Solutions for the Antarctic Circumpolar Current and Its Associated Overturning Circulation. *J. Phys. Oceanogr.*, **33**, 2341–2354, doi:10.1175/1520-0485(2003)033<2341:RSFTAC>2.0.CO;2.

Menemenlis, D., J. Campin, P. Heimbach, C. Hill, T. Lee, A. Nguyen, M. Schodlok, and H. Zhang, 2008: ECCO2: High resolution global ocean and sea ice data synthesis. *Mercator Ocean Q. Newslett.*, **31**, 13–21.

Nishikawa, S., H. Tsujino, K. Sakamoto, and H. Nakano, 2013: Diagnosis of water mass transformation and formation rates in a high-resolution GCM of the North Pacific. *J. Geophys. Res. Oceans*, **118 (3)**, 1051–1069, doi:10.1029/2012JC008116.

Noori, R., F. Tian, R. Berndtsson, M. R. Abbasi, M. V. Naseh, A. Modabberi, A. Soltani, and B. Kløve, 2019: Recent and future trends in sea surface temperature across the persian gulf and gulf of oman. *PLoS ONE*, **14 (2)**.

Patlakas, P., C. Stathopoulos, H. Flocas, C. Kalogeri, and G. Kallos, 2019: Regional climatic features of the arabian peninsula. *Atmosphere*, **10 (4)**, doi:10.3390/atmos10040220.

Pous, S., P. Lazure, and X. Carton, 2015: A model of the general circulation in the Persian Gulf and in the Strait of Hormuz: Intraseasonal to interannual variability. *Cont. Shelf Res.*, **94**, 55–70, doi:10.1016/j.csr.2014.12.008.

Reynolds, M. R., 1993: Physical oceanography of the Gulf, Strait of Hormuz, and the Gulf of Oman—Results from the Mt Mitchell expedition. *Mar. Pollut. Bull.*, **27**, 35–59, doi:10.1016/0025-326X(93)90007-7.

Rocha, C. B., T. K. Chereskin, S. T. Gille, and D. Menemenlis, 2016: Mesoscale to Submesoscale Wavenumber Spectra in Drake Passage. *J. Phys. Oceanogr.*, **46 (2)**, 601–620, doi:10.1175/JPO-D-15-0087.1.

Sadrinasab, M., and J. Kämpf, 2004: Three-dimensional flushing times of the Persian Gulf. *Geophys. Res. Lett.*, **31 (24)**, L24 301, doi:10.1029/2004GL020425.

Schott, F. A., and J. P. McCreary, 2001: The monsoon circulation of the Indian Ocean. *Prog. Oceanogr.*, **51 (1)**, 1–123, doi:10.1016/S0079-6611(01)00083-0.

Shirvani, A., M. J. Nazemosadat, and E. Kahya, 2015: Analyses of the Persian Gulf sea surface temperature: prediction and detection of climate change signals. *Arab J Geosci.*, **8**, 2121–2130.

Smith, W. H. F., and D. T. Sandwell, 1997: Global seafloor topography from satellite altimetry and ship depth soundings. *Science*, **277**, 1956–1962.

Speer, K., and E. Tziperman, 1992: Rates of Water Mass Formation in the North Atlantic Ocean. *J. Phys. Oceanogr.*, **22 (1)**, 93–104, doi:10.1175/1520-0485(1992)022<0093:ROWMFI>2.0.CO;2.

Swift, S. A., and A. S. Bower, 2003: Formation and circulation of dense water in the Persian/Arabian Gulf. *J. Geophys. Res.*, **108 (C1)**, 3004, doi:10.1029/2002JC001360.

Thoppil, P. G., and P. J. Hogan, 2010: A Modeling Study of Circulation and Eddies in the Persian Gulf. *J. Phys. Oceanogr.*, **40 (9)**, 2122–2134, doi:10.1175/2010JPO4227.1.

Torres, H. S., P. Klein, D. Menemenlis, B. Qiu, Z. Su, J. Wang, S. Chen, and L.-L. Fu, 2018: Partitioning Ocean Motions Into Balanced Motions and Internal Gravity Waves: A Modeling Study in Anticipation of Future Space Missions. *J. Geophys. Res. Oceans*, **123 (11)**, 8084–8105, doi:10.1029/2018JC014438.

Tziperman, E., 1986: On the Role of Interior Mixing and Air-Sea Fluxes in Determining the Stratification and Circulation of the Oceans. *J. Phys. Oceanogr.*, **16 (4)**, 680–693, doi:10.1175/1520-0485(1986)016<0680:OTROIM>2.0.CO;2.

Walin, G., 1982: On the relation between seaâĂŘsurface heat flow and thermal circulation in the ocean. *Tellus*, **34**, 187–195, doi:10.1111/j.2153-3490.1982.tb01806.x.

Wang, J., L. Fu, B. Qiu, D. Menemenlis, J. Farrar, Y. Chao, A. Thompson, and M. Flexas, 2018: An observing system simulation experiment for the calibration and validation of the surface water ocean topography sea surface height measurement using in situ platforms. *J. Atmos. Oceanic Technol.*, **35**, 281–297, doi:10.1175/JTECH-D-17-0076.1.

Xue, P., and E. A. B. Eltahir, 2015: Estimation of the heat and water budgets of the Persian (Arabian) Gulf using a regional climate model. *J. Clim.*, **28 (13)**, 5041–5062, doi:10.1175/JCLI-D-14-00189.1.

Yao, F., and W. E. Johns, 2010: A HYCOM modeling study of the Persian Gulf: 2. Formation and export of Persian Gulf Water. *J. Geophys. Res. Oceans*, **115 (C11)**, doi:10.1029/2009JC005788.

LIST OF FIGURES

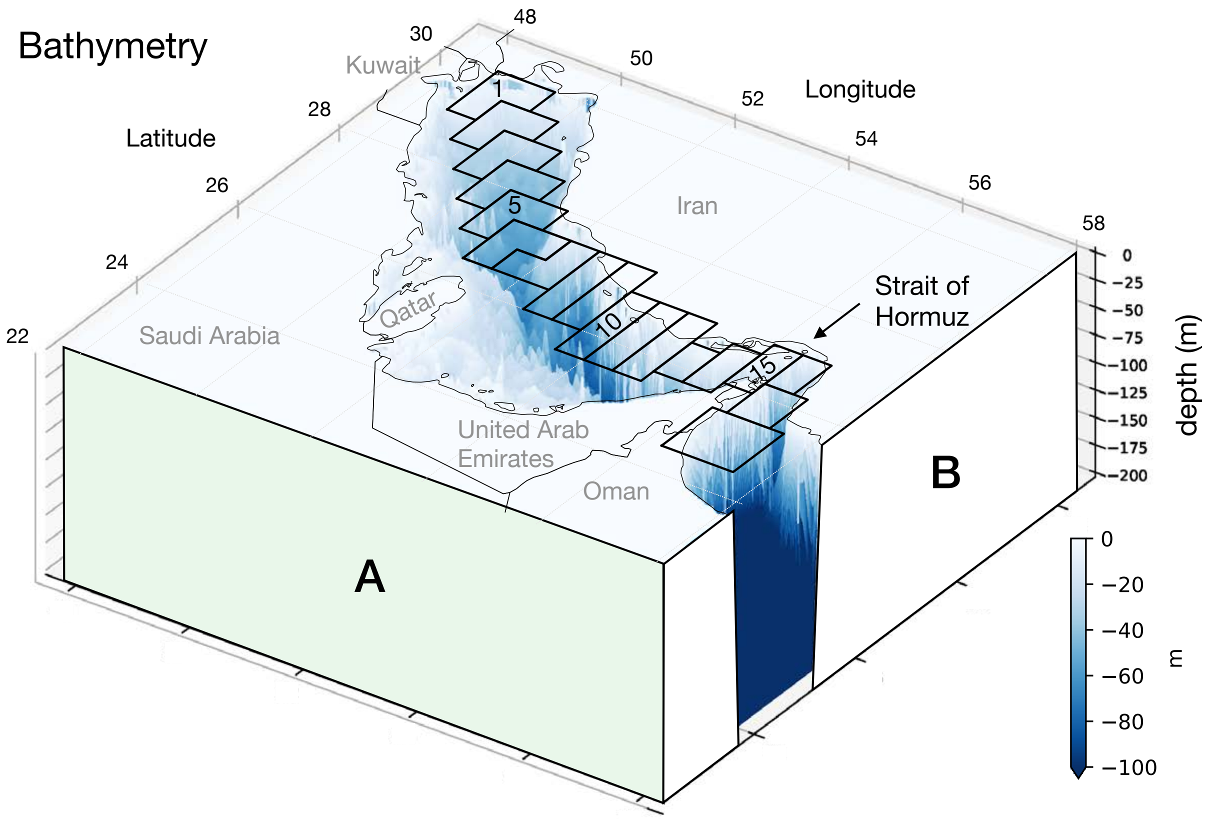

FIG. 1. The geography and bathymetry (shading in blue) of the Gulf of Arabia, together with the surrounding countries and the Strait of Hormuz marked. Eighteen black boxes, adopted from Figure 2 in (Swift and Bower 2003), are the regions over which spatial averages of in-situ observations and model results are compared. A and B indicate the section for the zonal and meridional streamfunction shown in Fig. 10.

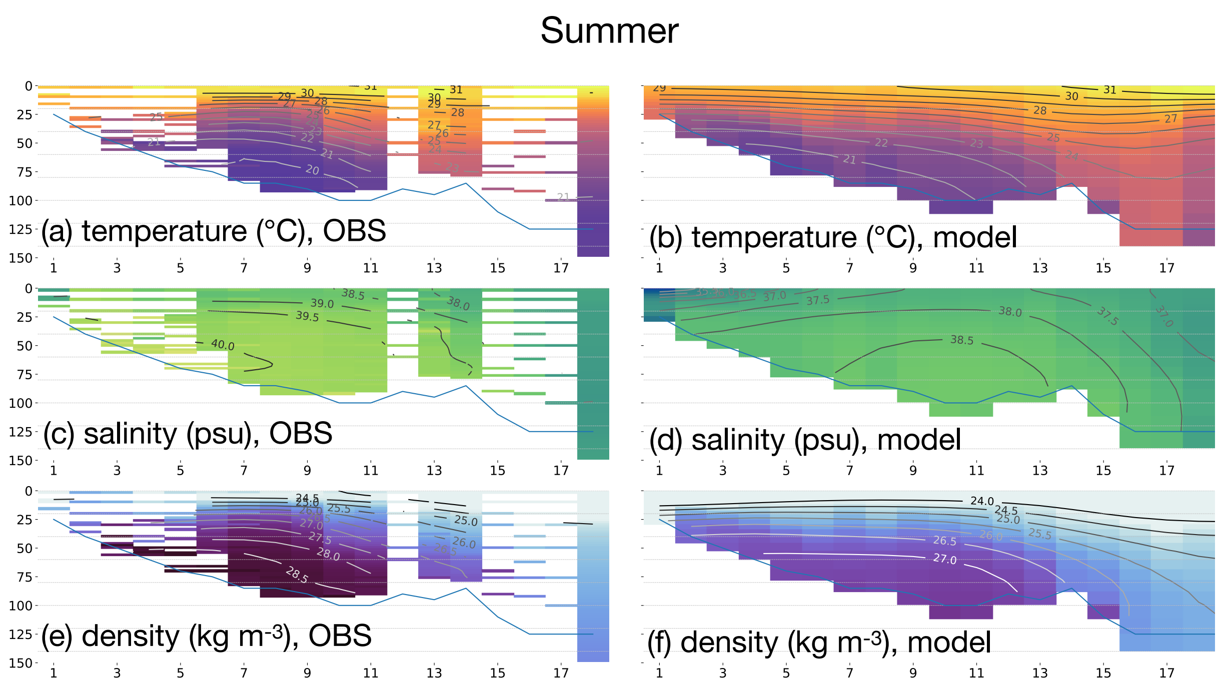

593 FIG. 2. Vertical section of (a,b) temperature, (c,d) salinity, and (e,f) density during summer in the boxes shown and labeled in Fig. 1. The observations on the left in (a,c,e) represent the mean of in-situ samples representative of the summer, July and August (adapted from Figure 7d in (Swift and Bower 2003)). The model solution on the right in (b,d,f) are spatial means over the same boxes again in summer but from June to August.

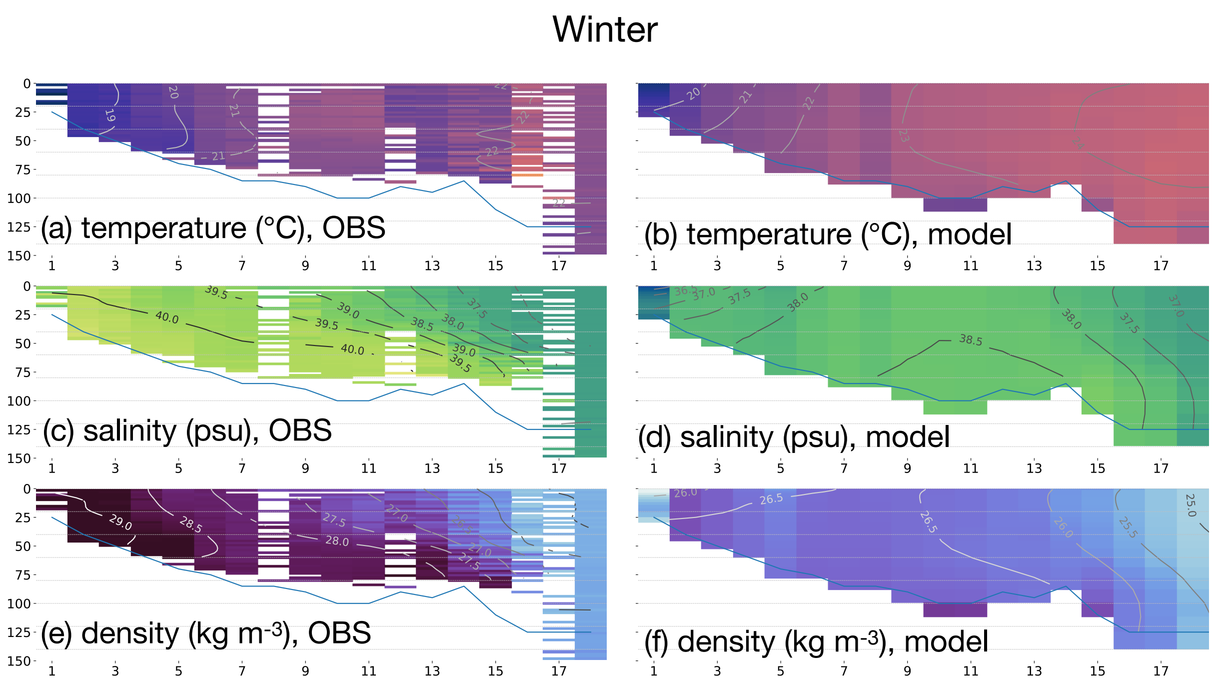

597 FIG. 3. As in Fig. 2 except that the observations are a mean over the winter period, January and February (as
598 shown in Figure 7a in (Swift and Bower 2003)). Observations are on the left, model on the right. The model
599 solution are a mean typical of the winter, from December to February.

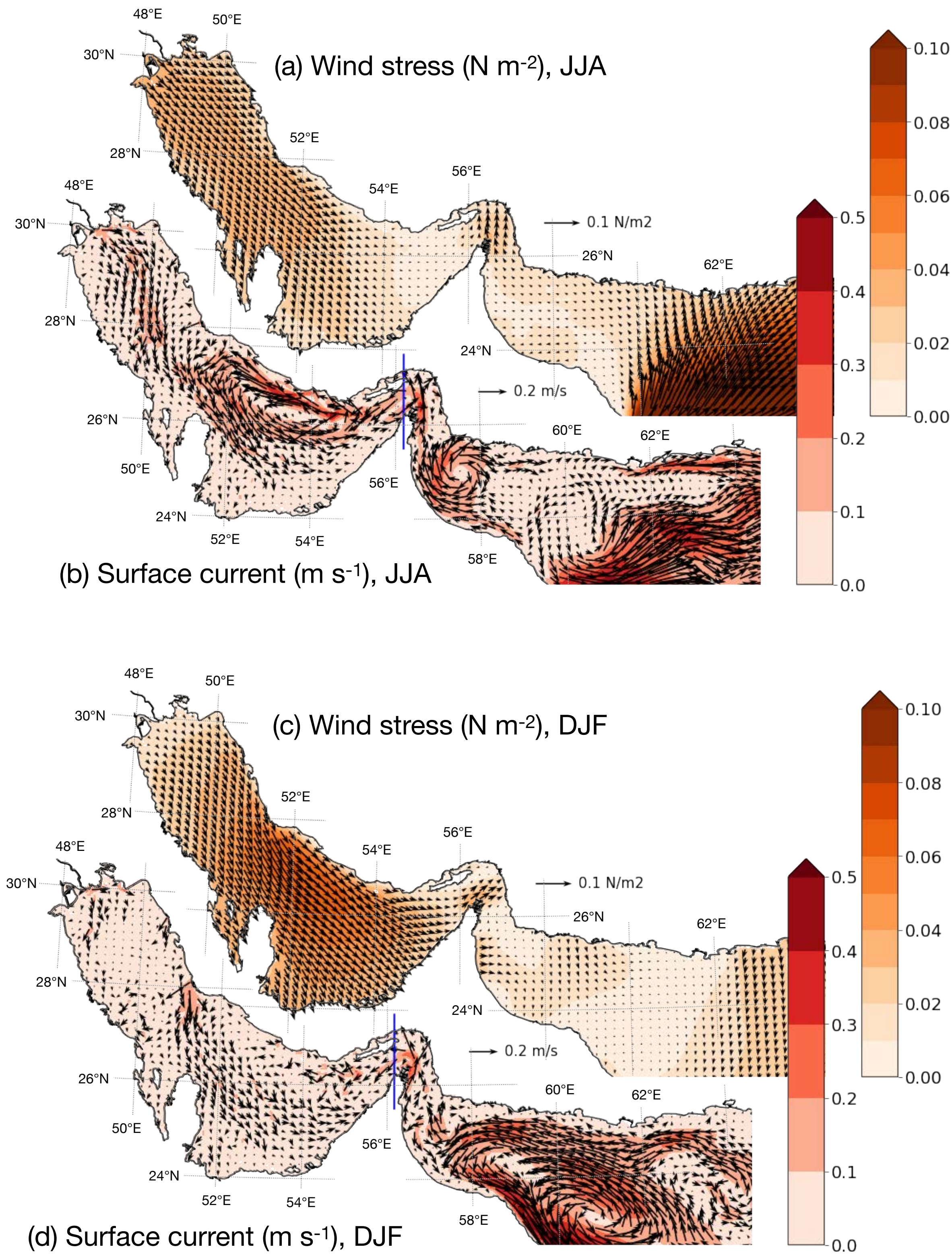

FIG. 4. (a,c) Wind stress (N m^{-2}) and (b,d) surface current (m s^{-1}) in (a,b) summer (June, July and August, JJA) and (c,d) winter (December, January and February, DJF). The shading represents the intensity of the flow whilst the arrows are also scaled by speed.

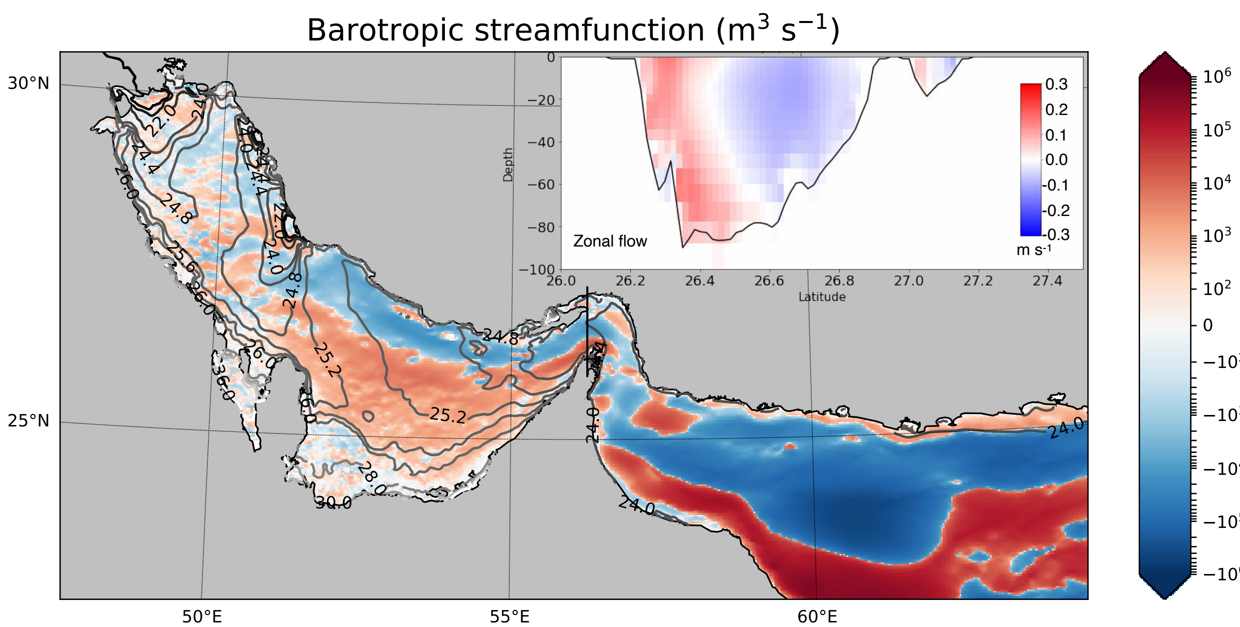

Fig. 5. Annually-averaged barotropic streamfunction plotted using a log scale (shading) along with outcropping isopycnals (contours). The inset shows a vertical section of the annually-averaged zonal velocity across the Strait of Hormuz with south on the left. There is counterclockwise circulation around a positive streamfunction. Positive zonal velocity in the inset is directed out of the Gulf.

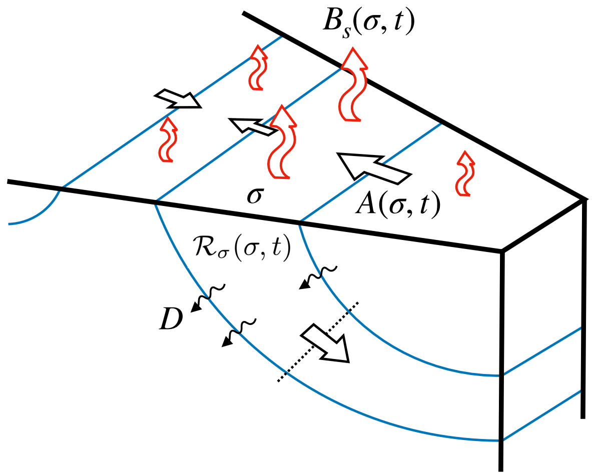

Fig. 6. Potential density surfaces, σ, outcropping at the sea surface within the Gulf (say) and extending back out in to the Gulf of Oman. The volume of fluid between adjacent σ surfaces, $\mathcal{R}_\sigma(\sigma,t)$, can be changed by the divergence of a diapycnal volume flux, $A(\sigma,t)$, normal to σ, which itself can be related to the air-sea buoyancy fluxes $\mathcal{B}_s$ and the diffusive buoyancy fluxes, D, acting on the σ surfaces that bound the volume, as expresses in Eqs (5) to (9).

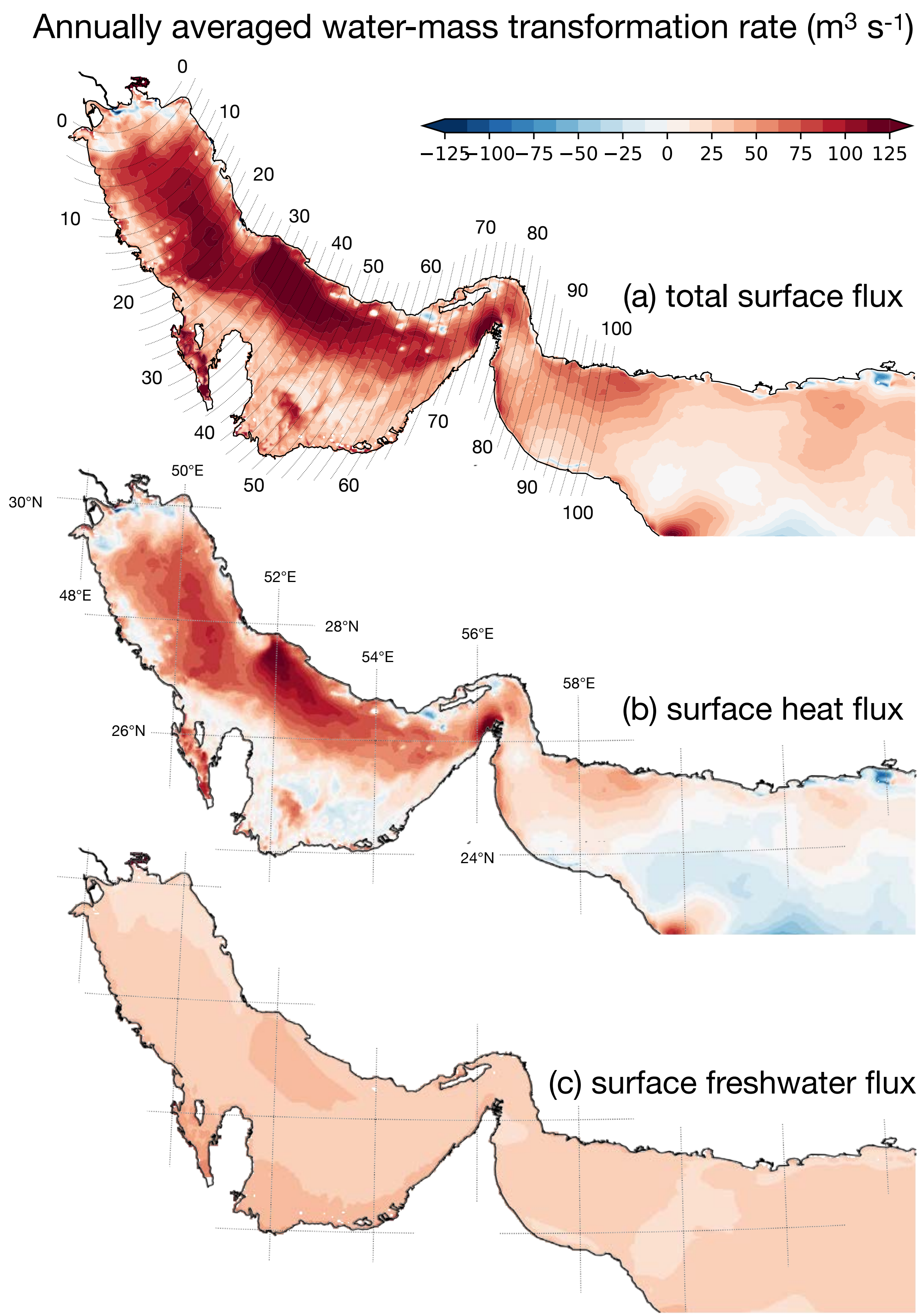

Fig. 7. (a) Annual-mean water-mass transformation rate, $F = \frac{\partial B_s(\sigma,t)}{\partial \sigma}$, in units of (m^3 s^{-1}), implied by air-sea

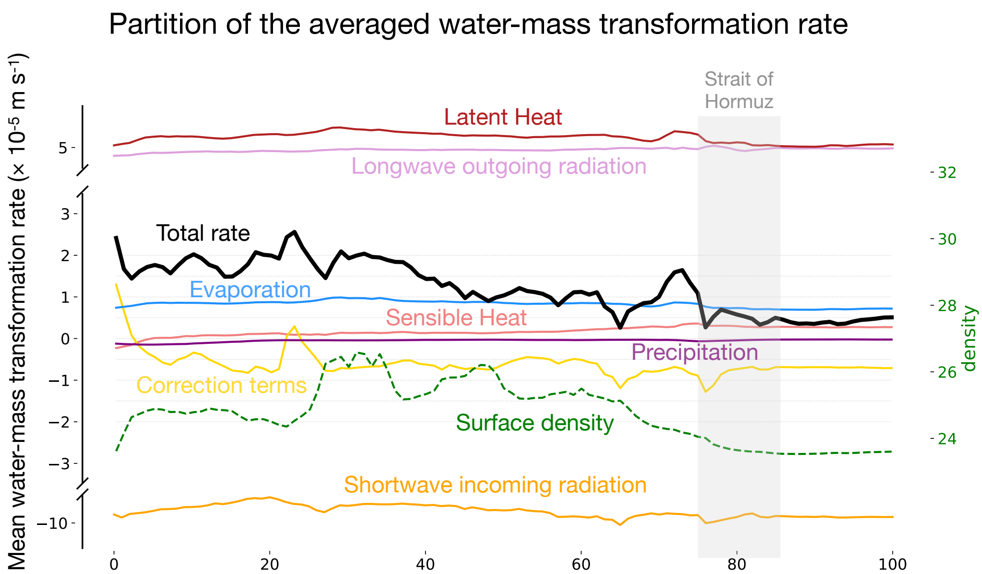

FIG. 8. (solid lines) Annual-mean water-mass transformation rate, $F(\sigma)$, computed from Eq.(6) using (9). The dashed line shows the surface density averaged in the sections numbered and shown in Fig. 7(a). The number along the x axis indicates the location of the section along the Gulf increasing eastwards. Positive values imply a tendency to induce a diapycnal volume transport directed toward higher densities. Points shallower than 20 m are excluded in the average. The contribution from river runoff is close to zero and hence not shown.

Annually averaged water-mass transformation rate (m^3 s^{-1})

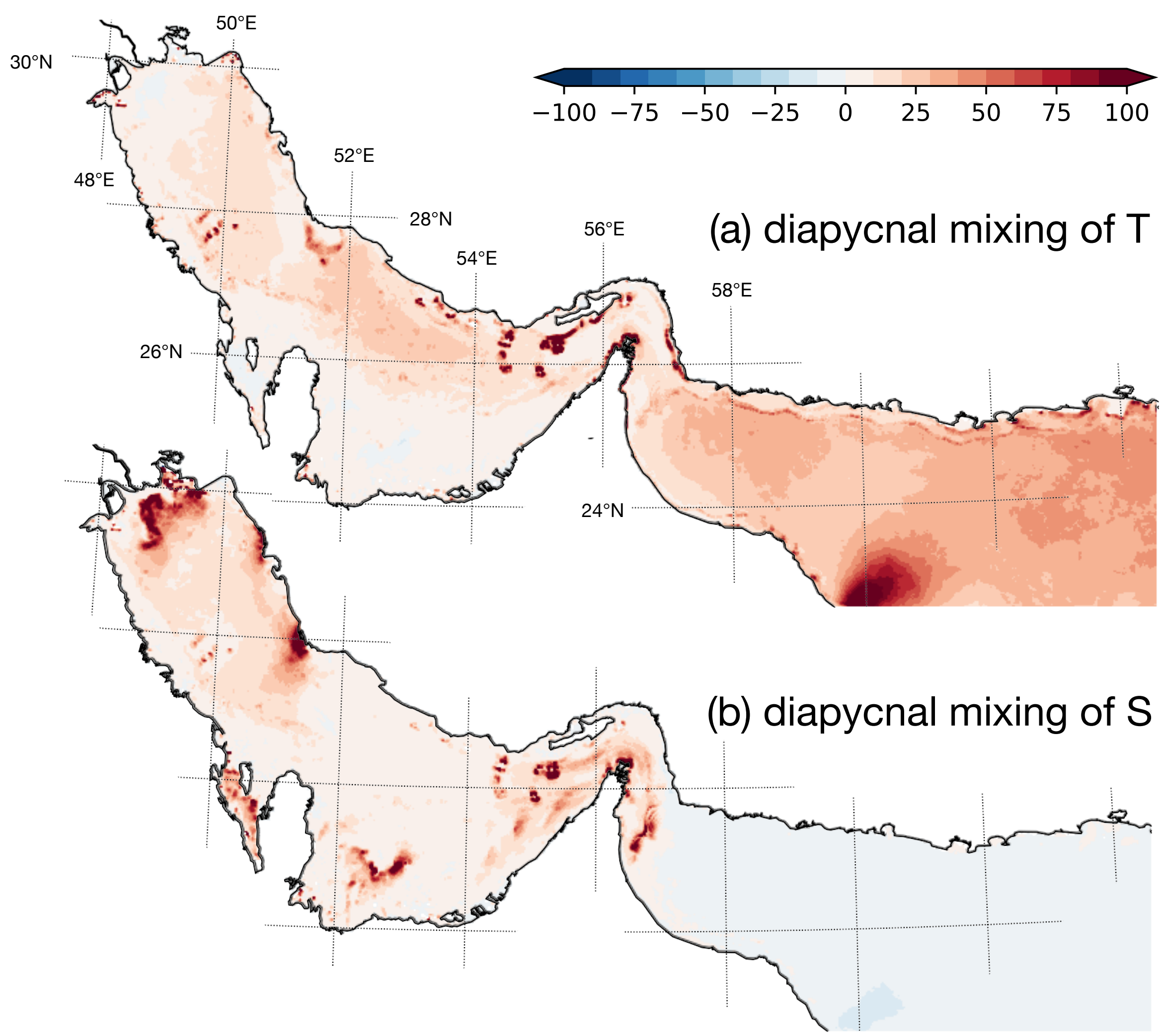

FIG. 9. Annual mean water-mass transformation rate contributed by diapycnal mixing of (a) temperature and (b) salinity integrated over the depth of the water column. The rate is weighted by the grid area. Note that the color scale is slightly different from Fig. 7, to enable details to be seen in the Gulf, although generally they are very much smaller than that due to air-sea interaction
.

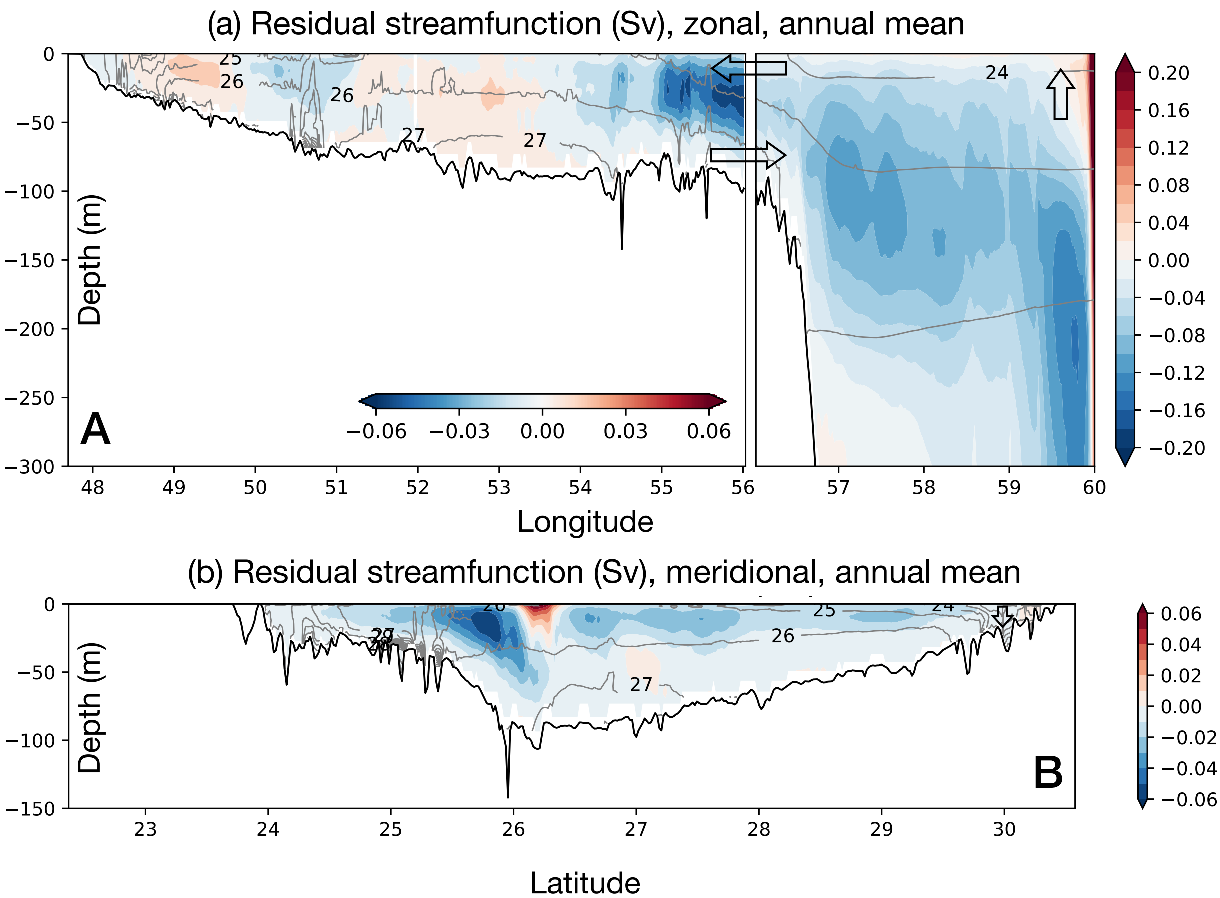

Fig. 10. Annually-averaged residual overturning streamfunction (shading) in (a) the zonal and (b) meridional directions parallel to A and B in Fig. 1, respectively. The Gulf and west of 60°E are considered in (a), and the Gulf (west of 56°) is considered in (b). Arrows in (a) represent the direction of the overturning circulation. Isopycnals are also plotted in gray with an interval of 1 kg m^{-3} in both (a) and (b). Blue shading represents anticlockwise circulation, red clockwise circulation. It should be noted that two different color scales (in Sverdrups) are used inside and outside of the Gulf in (a).

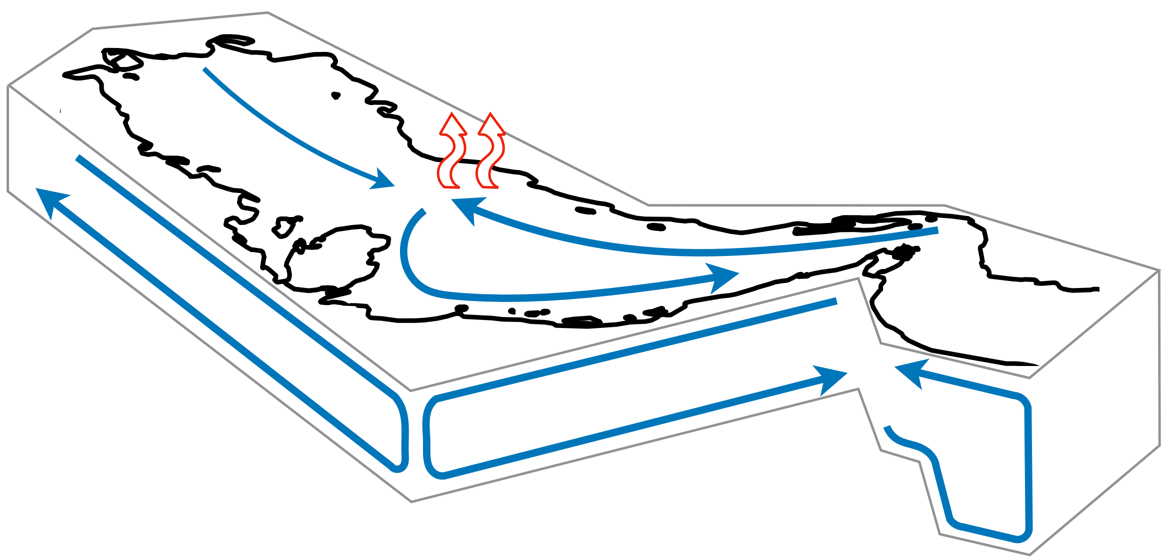

Fig. 11. A schematic diagram depicting the overturning circulation and water-mass transformation processes acting in the Gulf. The positive water-mass transformation rate due to surface fluxes (red curvy arrows) shapes the surface flow and overturning circulations.